Tests of Various Numerical Algorithms Applied to a Simple Trace Constituent Air Transport Problem

J. D. MAHLMAN AND R. W. SINCLAIR
Geophysical Fluid Dynamics Laboratory, NOAA
Princeton University
Princeton, New Jersey

I. INTRODUCTION

There are many problems in environmental science where a central concern is the manner in which a trace constituent is transported by a moving fluid. Some important examples are: global-scale transports of natural and anthropogenic tracers in the atmosphere and ocean, regional air pollution dispersion, river and lake pollution movement, and marine transport of pollutants in estuaries and coastal regions.

In each of these problems, a profitable approach has been to attempt simulation of tracer behavior by various numerical techniques. In many circumstances, it has proved to be useful to employ simplified empirical models that are designed to reproduce the overall behavior shown in a given set of data. Such an empirical model may often give satisfactory results for many problems but normally no attempt is made to simulate the actual transport mechanisms involved. An advantage of such an approach is that the calculations are normally not very demanding computationally. However, one of the hazards of such empirical methods is that it is not always evident that the model is applicable to problems or circumstances other than the one for which the model was empirically calibrated.

Another approach increasingly being employed involves attempts to calculate the tracer fluxes explicitly (e.g., Hunt and Manabe, 1968; Mahlman, 1973; Lawrence Livermore Laboratory, 1974; Cunnold et al., 1975). To perform such a calculation, it is necessary to know the tracer-transporting flow field with sufficient accuracy. In principle, this flow field can be specified from actual data or can be theoretically predicted through the use of hydrodynamic models. Once this has been accomplished, the problem then becomes one of solving the appropriate trace constituent continuity equation to the desired level of accuracy. Successful solution of such a problem usually requires special care in the formulation of three parts of the problem: transport by the known or resolved flow field, transport on scales below the chosen resolution of the problem, and addition or loss by various chemical or physical mechanisms. In most problems, however, processes in these various categories rarely operate independently of each other. For example, chemical processes can be highly dependent upon the mixing of constituents produced by the resolved and subscale transports. However, before addressing these problems of interactions, it is first necessary that the behavior of the given process be understood when it is isolated from other parts of the system. Otherwise, distortions or imperfections in the individual process also interact with other parts of the complex system.

No attempt will be made to address the interaction problem directly. The attempt instead will be to investigate some of the difficulties associated with an isolatable subset of the problem. The problem chosen is the calculation of transport (advection) of a trace constituent by a simple large-scale flow field. This calculation is common to all direct attempts to account for large-scale transport of trace constituents irrespective of the specific nature of the problem. In this context, it should be pointed out that even the simple empirical models used by many investigators result from a decision to account for the advection process in an indirect manner.

II. DEFINITION OF THE PROBLEM

In order to establish the problem in a straightforward manner, it is instructive to begin by writing the trace constituent continuity equation as

$$\frac{dR}{dt} = P - L + \nabla\cdot(k_m \nabla R) \qquad (1)$$

where R is the trace constituent mixing ratio (tracer density divided by carrier fluid density), P and L are the chemical-physical production and loss of R, respectively, V is the 3-dimensional gradient operator, k_m is the coefficient of molecular diffusivity, and t is time. The substantial derivative of R (dR/dt) represents the time rate of change of R following an infinitesimal fluid parcel.

For problems of concern here, the molecular diffusivity is far too small to have any direct influence on the tracer dispersion. This does not imply that the irreversible mixing due to molecular diffusion is physically unimportant. It just indicates that molecular diffusion is not important except when the gradients of R are extremely large. This can only occur at size scales so small as to be unresolvable by any practical model. A frequently employed "cure" for this difficulty is to choose a much larger coefficient of diffusivity that is consistent with the resolution chosen for a particular calculation. Inclusion of such an "eddy diffusion" coefficient in a model calculation hopefully accounts for the irreversible mixing that is actually only accomplished on molecular scales in nature. As yet no fully satisfactory ways exist to include such effects in a model calculation. However, virtually all geophysical fluid flows contain shearing and stretching of fluid elements that lead to the

requirement of including some kind of transfer to scales smaller than those resolved by the chosen model.

In this paper, the previously mentioned difficulty will be circumvented in part by considering only the transport by an exceedingly simple flow, that is, one in which there is no obvious short-term physical requirement for inclusion of transport effects on scales below the chosen grid resolution.

Consider the simple case where $dR/dt = 0$, and $\nabla \cdot \vec{V}_3 = 0$ ($\vec{V}_3$ is the three-dimensional velocity vector). Physically, this can be imagined as the transport of a trace constituent in a homogeneous fluid (such as water) in which no chemical-physical production or removal of R is acting. For this case, after performing an Eulerian expansion of dR/dt, Eq. 1 becomes

$$\frac{\partial R}{\partial t} = - \nabla \cdot \vec{V}_3 R = - \frac{\partial uR}{\partial x} - \frac{\partial vR}{\partial y} - \frac{\partial wR}{\partial z} \qquad (2)$$

where u, v, and w are the velocity components in the x, y, and z cartesian coordinate directions, respectively. To further simplify the problem and eliminate the immediate need for including subgrid scale transfer, assume that $v = w = \partial u/\partial x = 0$. This leads to the apparently trivial linear equation

$$\frac{\partial R}{\partial t} = - u_o \frac{\partial R}{\partial x} \qquad (3)$$

Here, u_o is a constant wind. The solution for this equation is that the initial tracer field is simply transported along the x axis at the flow speed u_o.

Once the initial tracer field has been defined and a numerical grid is established, the only possible sources of error in the numerical solution are the truncation errors that arise from approximating the space and time derivatives in Eq. 3 by various numerical algorithms. The investigation of the effects of these truncation errors is the main purpose of this study.

The initial condition chosen for these tests is a "wedge" of inert tracer with the following definition relative to a dimensionless coordinate defined such that $x' = x/\Delta x$, and $\Delta x' = 1$:

$$R = 0 \text{ for } x' \leq -5 \text{ or } x' \geq 5$$

$$R = 1 + \frac{x'}{5} \text{ for } -5 \leq x' \leq 0 \qquad (4)$$

$$R = 1 - \frac{x'}{5} \text{ for } 0 \leq x' \leq 5$$

The initial field is thus a one-dimensional wedge of tracer ten grid increments in width. Figure 1 shows this initial tracer mixing ratio distribution expressed in arbitrary normalized units. From a finite difference viewpoint, this is a somewhat difficult problem because the x' derivatives of R are not continuous throughout the domain. However, this is thought to be a meaningful problem because it approximately represents the type of distribution that could result from a local source of tracer or one that could appear in a tracer field due to a complex flow stretching or shearing a tracer field. This wedge-shaped tracer distribution has become almost a standard test case for advection problems, as it has been previously used in studies by Crowley (1968), Molenkamp (1968), Burnstein and Mirin (1970), and Orszag (1971).

An attractive feature of the simple initial condition expressed in Eq. 4 is that domain integrals ($\int (\,) dx'$) can then be determined from the analytic solution. For the simple problem expressed by Eq. 3, the following domain integrals are conserved for all time, i.e:

$$\frac{\partial}{\partial t} \int R dx' = 0 \qquad (5)$$

$$\frac{\partial}{\partial t} \int R^2 dx' = 0 \qquad (6)$$

$$\frac{\partial}{\partial t} \int R^4 dx' = 0 \qquad (7)$$

$$\frac{\partial}{\partial t} \int \left(\frac{\partial R}{\partial x'} \right)^2 dx' = 0 \qquad (8)$$

$$\frac{\partial}{\partial t} \int \left(\frac{\partial^2 R}{\partial x'^2} \right)^2 dx' = 0 \qquad (9)$$

These integrals can be numerically evaluated by summing over the total number of grid points in the domain (NI). It is not

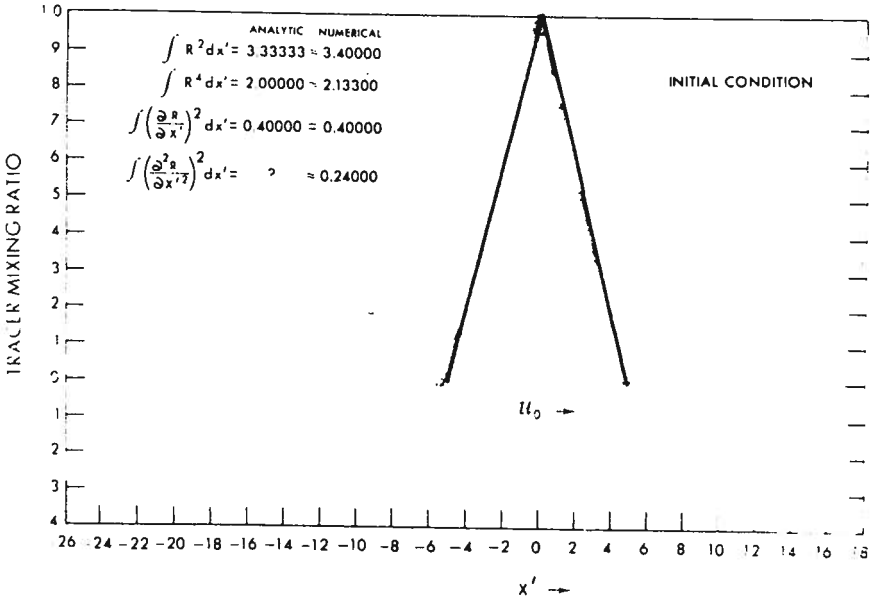

FIGURE 1. Initial condition for wedge advection problem at t = 0, centered at x' = 0. Ordinate is tracer mixing ratio in arbitrary units and abscissa is dimensionless distance such that $\Delta x' = 1.0$. Analytic and finite sum evaluation of various integrals are given at upper left. The various integrals shown are approximated numerically by $\int R^\beta dx' \approx \sum_{i=1}^{NI} R^\beta$ (β is any power):

$$\int \left(\frac{\partial R}{\partial x'}\right)^2 dx' \approx \sum_{i=1}^{NI} (R_{i+1} - R_i)^2; \int \left(\frac{\partial^2 R}{\partial x'^2}\right)^2 dx' \approx$$

$$\sum_{i=1}^{NI} (R_{i+1} - 2R_i + R_{i-1})^2.$$

obvious, however, that the numerical analogs of these integrals will, in fact, be preserved during the course of a numerical integration of Eq. 3. It is thus of interest to monitor the behavior of the numerical analogs of these integrals as a means of evaluating the relative merits of the various algorithms tested.

The first integral (5) expresses conservation of tracer mixing ratio for this problem. All of the algorithms tested in this study conserve the tracer integral to the computer roundoff accuracy. Thus, the behavior of the integral (5) is of no further direct interest.

The analytic evaluations of each of the integrals (6) through (9) along with their numerical equivalents are given in Figure 1. Integral (6) expresses conservation of the mean square of the tracer. It is of great interest because diffusive effects act to damp this quantity. All of the advection algorithms tested here are regarded as "essentially nondiffusive," that is, they do not contain large diffusive effects implicitly in the numerical algorithm. This is primarily due to the authors' philosophical preference to have a direct control on the diffusive effects through explicitly included diffusion terms. A prominent example of an "essentially diffusive" scheme is the so-called first-order upstream differencing technique. Its difficulties were pointed out in an analysis by Molenkamp (1968).

The higher-order integrals (7) through (9) possess quite different properties. Integral (7) tends to measure ability of a numerical scheme to maintain the peak mixing ratios. Note in Figure 1 that the analytic and numerical evaluations of Eq. 7 for the initial condition differ slightly. Integral (8) measures the growth or decay of local tracer gradients. Figure 1 shows that the analytic and numerical evaluations agree exactly. Integral (9) measures the rate of growth or decay of tracer curvature. The analytic evaluation of Eq. 9 is undefined because of the presence of derivative discontinuities in the initial condition. The numerical evaluation in Figure 1 is well defined.

In a more general context, it should be noted that the integrals (5) through (7) are analytically conserved in more complex source-free, nondiffusive flows, whereas the integrals (8) and (9) are not guaranteed to be conservative. If gradient-reducing diffusion terms are not included in calculations with more complicated flows, the integrals (8) and (9) tend to increase with time. This can result either from numerical distortions or from a physically real cascade to smaller spatial scales. In such calculations, it is often difficult to establish which of these two effects is dominant.

The foregoing points out an advantage of performing test calculations in a simple flow where the integrals (8) and (9) are analytically conserved. If, in such cases, these integrals

increase with time in the numerical integration, it can only have occurred due to a spurious source of "noise" in the calculation. This eventually leads to the requirement of adding extra damping effects to keep this spurious growth from irreversibly contaminating the calculation. Thus the behavior of integrals (8) and (9) are of particular interest in the numerical experiments to be described.

III. DESCRIPTION OF THE NUMERICAL ALGORITHMS TESTED

The numerical schemes selected for testing are all of general applicability, and none of them have been contrived to perform well on this particular problem. In addition, all of the schemes tested are simple in that they use explicit time differencing. Depending on the stability requirements for a given algorithm, either a forward (Euler) step or a centered (leapfrog) step is used. The interpretation of the problem is simplified by writing Eq. 3 in the nondimensional forms:

$$R_{i,\tau+1} = R_{i,\tau} - \alpha \left(\frac{\partial R}{\partial x'}\right)_{i,\tau} \quad \text{(Euler)} \tag{3a}$$

$$R_{i,\tau+1} = R_{i,\tau-1} - 2\alpha \left(\frac{\partial R}{\partial x'}\right)_{i,\tau} \quad \text{(leapfrog)} \tag{3b}$$

where $\alpha = u_o \, \Delta t/\Delta x$, i represents the position in the x' grid, and $\tau-1$, τ, and $\tau+1$ represent successive time levels. In the various tests, a leapfrog time step is used for the centered polynomial, cubic spline, and pseudo-spectral algorithms, while an Euler step is employed for the quasi-Lagrangian algorithms.

A. Centered Polynomial Algorithms

The first three schemes to be tested can be derived by assuming that the function R can be represented by polynomials in terms of x'. By employing a Taylor series expansion about the point i, the derivative in Eq. 3a and Eq. 3b can be approximated by

$$\left(\frac{\partial R}{\partial x'}\right)_{i,\tau} \approx \left[A(R_{i+1} - R_{i-1}) + B(R_{i+2} - R_{i-2})\right]_\tau \tag{10}$$

where A and B are constant coefficients. If the spatial distribution of R can be completely represented by a second-order polynomial, the coefficients

$$A = \frac{1}{2}, \; B = 0 \quad \text{(centered second-order calculation)}$$

give an exact calculation of $\partial R/\partial x'$ in Eq. 10. If the function can be fully described by a fourth-order polynomial, the coefficients

there is a −

$$A = \frac{2}{3}, \; B = \frac{1}{12} \quad \text{(centered fourth-order derivative)}$$

sign missing here

determine $\partial R/\partial x'$ exactly in Eq. 10. For a fourth-order polynomial, the coefficients

$$A = \frac{5}{8}, \; B = \frac{1}{16} \quad \text{(centered fourth-order flux divergence)}$$

give an exact calculation of the flux divergence $(u_o R_{i+1/2} - u_o R_{i-1/2})_\tau$ between i + 1/2 and i - 1/2. Such a formulation can be useful when the R value at point i is conceived as an integral over the interval i - 1/2 to i + 1/2. For examples of such an integral approach as applied to more complex problems, see Bryan (1966) and Kurihara and Holloway (1967).

B. Quasi-Lagrangian Algorithms

One approach to the problem of numerically solving Eq. 3 involves the observation that an individual fluid parcel conserves its mixing ratio in this simple system. The method is simply to calculate where the parcel at the grid point i, and at time $\tau + 1$, should have been at the previous time step - when moving at the speed u_o. This location is α grid increments away from the point i, $\tau + 1$. If $\alpha < 1$, the predicted value of $R_{i,\tau+1}$ is determined simply by interpolating from the array of R values at time step τ (Krishnamurti, 1962).

If α is small so that the value to be interpolated is near the point i, $\tau + 1$, use of the Stirling polynomial interpolation

formula provides a good estimate of the predicted value for $R_{i,\tau+1}$. The Stirling formula algorithm can be written to fourth-order accuracy as

$$R_{i,\tau+1} = R_{i,\tau} + \left[-\frac{\alpha}{2}(R_{i+1} - R_{i-1}) + \frac{\alpha^2}{2}(R_{i+1} - 2R_i + R_{i-1}) - \frac{\alpha}{12}(\alpha^2 - 1)(R_{i+2} - 2R_{i+1} + 2R_{i-1} - R_{i-2}) + \frac{\alpha^2}{24}(\alpha^2 - 1)(R_{i+2} - 4R_{i+1} + 6R_i - 4R_{i-1} + R_{i-2}) \right]_\tau \quad (11)$$

After manipulation, Eq. 11 is identical to the fourth-order advection scheme of Crowley (1968). If the last two terms of Eq. 11 are dropped, the resulting algorithm becomes equivalent to the Lax-Wendroff (1960) scheme for constant u (Richtmeyer, 1963). It is also the same as the second-order schemes used by Leith (1965), Crowley (1967, 1968), and Mathur (1970).

Other interpolation schemes in quasi-Lagrangian algorithms are also possible. For example, if α is closer to 0.5 than 0.0, a more logical choice might be Bessel's polynomial interpolation formula, because it is designed to be more accurate midway between grid points, whereas the Stirling formula is more accurate near grid points.

C. Cubic Spline Algorithm

Another important approach to the advection problem has been to fit a smooth cubic spline function to the R field in the vicinity of the grid point i. The cubic spline is a piecewise continuous cubic polynomial between the grid points i and i-1, with continuous first and second derivatives everywhere. The values of $\partial R/\partial x'$ in Eq. 3b can be obtained at each grid point i by solving a set of NI simultaneous linear algebraic equations. For details on spline techniques, see for example, de Boor (1962), Ahlberg et al. (1965, 1967), Fritsch (1971), and Price and MacPherson (1973). In the spline scheme tested here, the derivatives were computed by including the influence of the R field at 10 points each side of the grid point i.

D. Pseudo-Spectral Algorithms

A proposal was advanced by Orszag (1972) that suggests a powerful method for solving Eq. 3b in a grid array. Simply expand the variable R at the grid points in terms of a predetermined set of basis functions and then differentiate the resulting series at each i point for substitution into Eq. 3b. The type and number of basis functions is dependent upon the physical problem and the accuracy desired.

In this study, trignometric functions are chosen to exploit the simple nature of the grid and the availability of the fast Fourier transform algorithm first developed by Cooley and Tukey (1965). Since the basic grid contains 256 points, the most wave numbers (n) that can be included is 128. To test the effects of wave number truncations, experiments are also run with n = 32.

E. Lagrangian Trajectory Algorithms

A superb method for solving Eq. 3 is to mark the initial field at a number of points with the appropriate initial mixing ratio and calculate the trajectories of the infinitesimal parcels by solving $dx/dt = u$ for each of the chosen points. Such a scheme reduces the problem addressed here to a trivial one. The position of each original parcel is simply $x_o + u_o(t - t_o)$, where $t - t_o$ is the total time elapsed after the initial time t_o. The mixing ratio thus always remains the same as that assigned to the original parcel.

The essence of this scheme has been employed for short range (hours to days) dispersion problems in the atmosphere for a number of years (for discussion and pertinent references see Reiter (1972)). For such shorter-range problems, this approach is very useful. For longer-range problems, however, a major disadvantage appears because of the scale cascade that arises from the stretching and shearing of fluid elements. When this occurs, the surface-to-mass ratio of a fluid volume tends to increase markedly. As a result, more and more "tagged" points are required to resolve the tracer field adequately. The only alternative to this is to devise some scheme for mixing between adjacent air parcels. This appears to be a cumbersome and uncertain process in the Lagrangian system. Thus Eulerian methods, such as those tested here, seem to be more advantageous for the more complicated longer-range problems.

IV. BOUNDARY CONDITIONS AND REGION SIZE

The basic number of grid points (NI) for this series of experiments is 256. In all experiments, cyclic continuity is imposed at the end points. This can be thought of as an endless series of the same problem or, alternatively, as movement around a circle. The numerical solutions to be emphasized in these experiments are after the initial field has been translated 15 wedge widths or 150 grid points. Thus the danger of self-contamination due to the limited region size is small for these experiments. For illustrative purposes, however, an example will be given for a 90 wedge width translation, which illustrates that self-contamination because of limited region size can at times be quite significant.

V. THE NEGATIVE MIXING RATIO PROBLEM

In transport problems of the kind examined here, truncation error in evaluating space and time derivatives almost inevitably leads to the prediction of negative mixing ratios at a number of grid points. The only exceptions to this appear to be in schemes that contain excessive damping (e.g., upstream differencing) or are "perfect" for this problem (e.g., Lagrangian trajectory methods). Since negative mixing ratios are not physically possible, their presence in a numerical solution can be a source of much difficulty. This is particularly true when significant tracer sources and sinks are included.

A reasonable approach to the negative mixing ratio problem is to demand that all mixing ratios be either zero or positive everywhere. In this work, the approach chosen is based upon the observation that low-order advection schemes tend to produce negative mixing ratios when small values of tracer are being advected into regions of much higher tracer values. It is called the method of "downstream borrowing" (Mahlman, 1973) for "filling" the "holes" of negative mixing ratio. Basically, after a time step $\tau + 1$ is completed, a negative R is filled back to zero by borrowing tracer from the downstream grid box in a tracer-conserving manner. In the event that the downstream grid box does not contain an adequate amount of tracer to prevent both boxes from becoming negative, the deficit is borrowed from the upstream grid box. In the higher-order schemes it is occasionally necessary to borrow tracer from the second grid boxes away from the negative value.

Although this filling process always acts to preserve the total tracer in the system, it systematically acts to reduce the mean square of the tracer (i.e., in integral (6), $\partial/\partial t \int R^2 dx' < 0$). This reduction occurs because a positive value and a negative value are both being reduced in absolute value during the filling process. Filling is thus equivalent to adding a special form of nonlinear diffusion to Eq. 3. Because of the frequent desirability of insuring that all mixing ratios be nonnegative in tracer transport problems, all schemes examined are executed with and without filling of negative mixing ratios. It should be pointed out that the "proper" choice of filling algorithm becomes less obvious as the order of the advection scheme increases. This is due to the increasing nonlocality of the mechanism for calculating derivatives with higher-order schemes.

VI. EXPERIMENTAL RESULTS

All experiments were run on the NI = 256 grid with $\tau = 0.3125$ and $\tau = 0.03125$. Normally, $\tau = 0.3125$ would appear to be a sufficiently small value to effectively suppress distortions due to time-truncation error. This is not always the case, however. For presentation of results, the $\tau = 0.3125$ experiments will be shown because they represent a more "typical" choice of time step in such problems. Results for the $\tau = 0.03125$ experiments will be shown when use of this shorter time step leads to significantly different results.

A. Polynomial Algorithms

Results from the standard second-order scheme of Eq. 10 with A = 1/2 and B = 0 are given in Figure 2. This figure shows rather dramatically the well-known errors of a second-order algorithm. The no-filling run shows a significant phase lag, an appreciable decrease in the maximum value, and a trail of nonphysical waves behind the wedge of tracer. The deepest hole is -0.34, over one-third of the magnitude of the original peak. This occurs in spite of the guaranteed conservation of the finite evaluations of $\int R^2 dx'$, $\int (\frac{\partial R}{\partial x'})^2 dx'$, and $\int (\frac{\partial^2 R}{\partial x'^2})^2 dx'$ by this algorithm. Note that $\int R^4 dx'$ shows a drastic decrease. An excellent analysis of the errors to be expected in second- and fourth-order polynomial schemes is given in Orszag and Israeli (1974).

Figure 2 shows that the experiment with filling leads to a complete suppression of the nonphysical waves behind the wedge. This occurs, however, at the expense of a large decrease in all the higher-order integrals.

Results from the fourth-order flux divergence algorithm of Eq. 10 with A = 5/8 and B = 1/16 are shown in Figure 3. This scheme shows a significant improvement over the previous one.

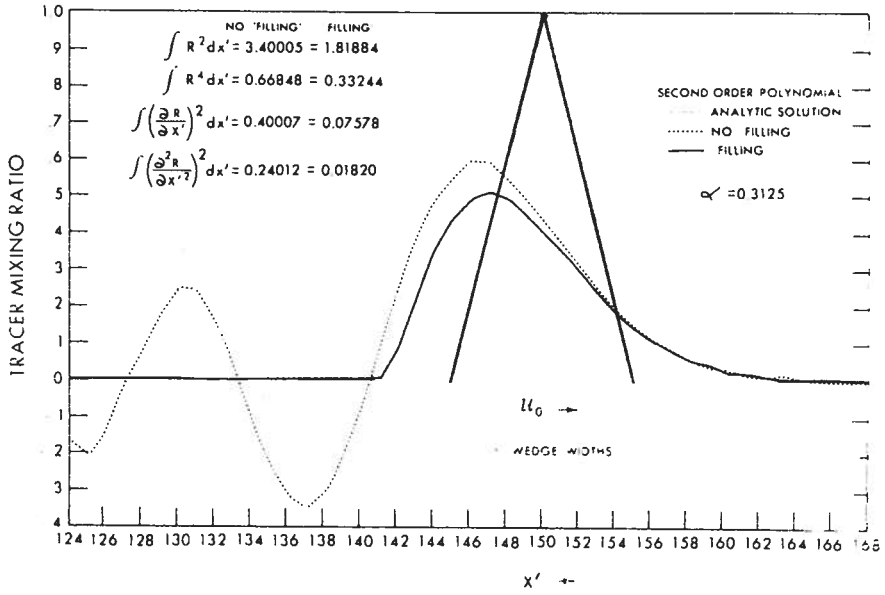

FIGURE 2. Analytic versus numerical solution after movement of 15 wedge widths for second-order polynomial algorithm with and without filling. Finite sum evaluations of various integrals are given at upper left for no-filling and filling cases (α = 0.3125).

It has a smaller phase lag, the peak is not diminished as much, and the deepest hole is somewhat smaller (-0.25).

The run with filling shows a secondary "bump" of tracer behind the main wedge. A bump phenomenon away from the main wedge appears in all higher-order schemes tested. It results from the progressive nonlocality of the computed derivatives and its interaction with filling as the order of accuracy is raised.

Figure 4 shows the result for the fourth-order derivative scheme of Eq. 10 with A = 2/3 and B = 1/12. The solution shows a marked improvement over the previous two schemes. The phase error is negligibly small (partly fortuitous, as will be shown later), the peak is more nearly preserved, the nonphysical waves are noticeably suppressed, and the deepest hole is now only -0.08.

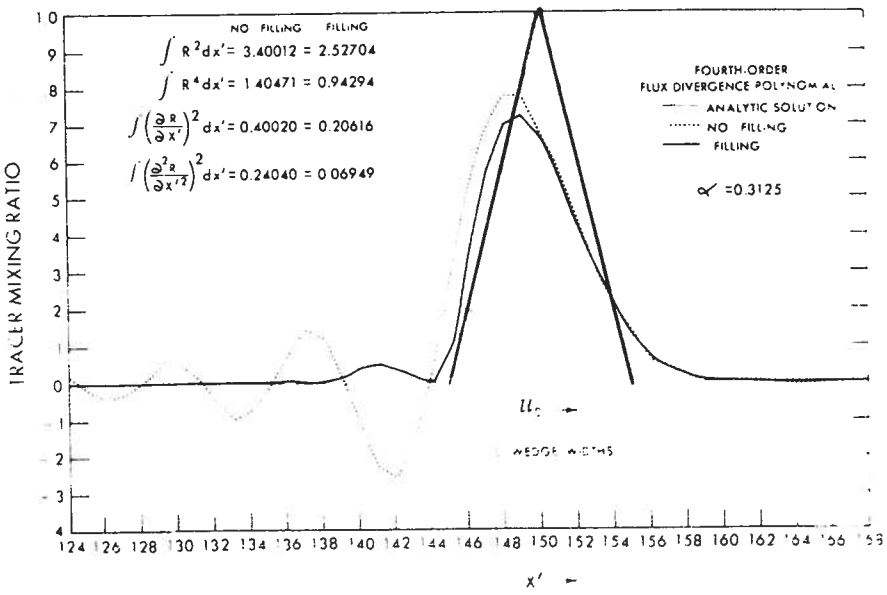

FIGURE 3. Same as Figure 2, except for fourth-order flux divergence polynomial algorithm.

The case with filling in Figure 4 also shows significant improvement over the previous two polynomial schemes. Less damping of all higher-order integrals is apparent. Note, however, that the trailing bump is larger than for the previous scheme.

B. Quasi-Lagrangian Algorithms

When the second-order quasi-Lagrangian algorithm using the first two terms within the brackets in Eq. 11 is applied to this problem, the results (not shown) are quite similar to those shown in Figure 2. The trail of nonphysical waves is somewhat smaller, and the scheme shows damping of higher-order integrals even without filling of negative mixing ratios.

The fourth-order quasi-Lagrangian results are given in Figure 5 and show overall characteristics similar to the

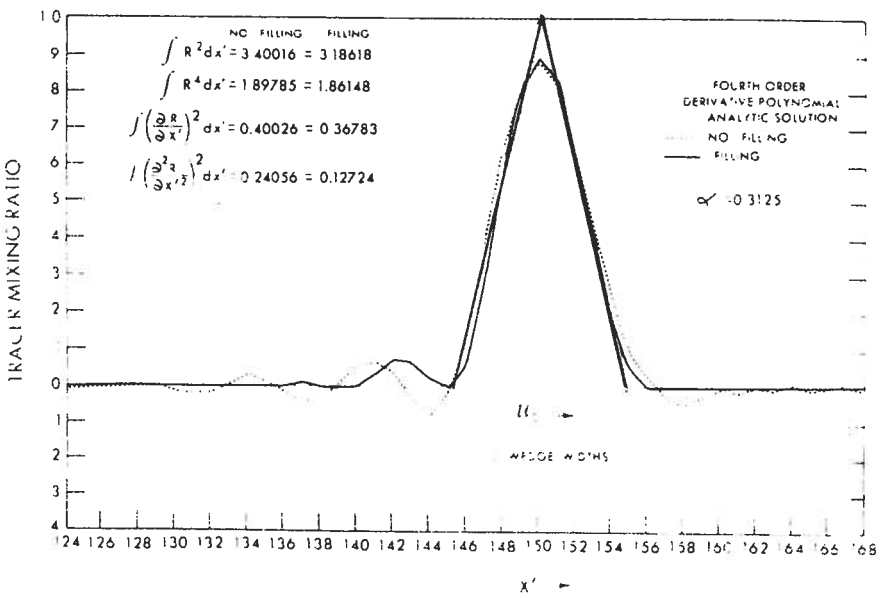

FIGURE 4. Same as Figure 2, except for fourth-order derivative polynomial algorithm.

centered fourth-order derivative results shown in Figure 4. No evidence of phase lag is present in this scheme, although the peak value is smaller and the deepest hole is larger than for the scheme shown in Figure 4. Note that this algorithm produces a systematic damping of all the listed integrals even before filling is applied.

Introduction of filling again leads to a secondary bump behind the wedge. Note in Figure 5 that $\int (\frac{\partial^2 R}{\partial x'^2})^2 dx'$ increases somewhat after imposing negative mixing ratio filling. This is interpreted as evidence that the filling effect introduces a weak amplification of some smaller-scale features in this higher-order scheme.

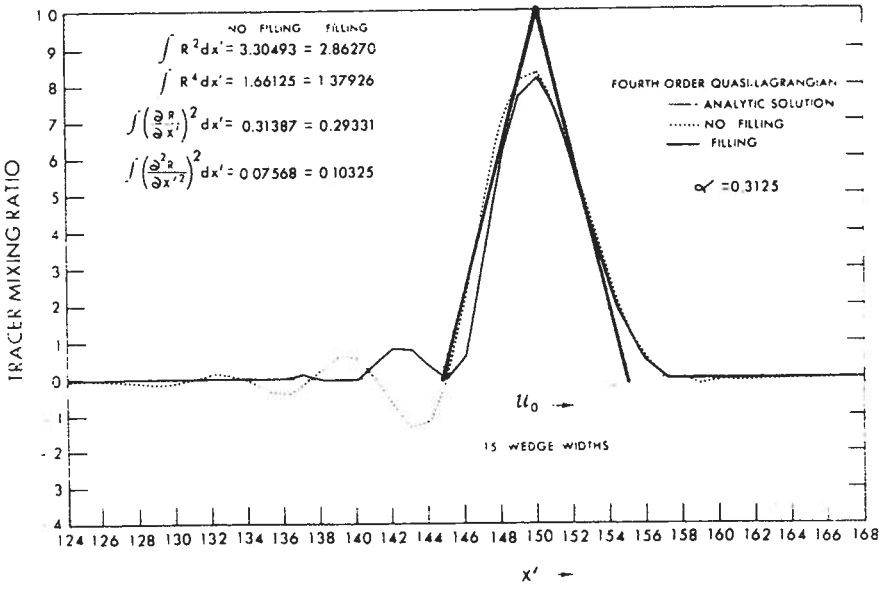

FIGURE 5. Same as Figure 2, except for fourth-order quasi-Lagrangian algorithm.

C. Cubic Spline Algorithm

The cubic spline results illustrated in Figure 6 show a general level of skill quite similar to the other fourth-order methods. There is evidence of a phase advance, however, instead of the phase lags shown earlier. The deepest hole is now in front of the wedge, rather than behind it as in previous schemes. This algorithm exhibits less damping of $\int R^4 dx'$ than the previous methods.

In the spline method, introduction of filling still damps $\int R^2 dx'$, but interestingly the integrals $\int R^4 dx'$, $\int (\frac{\partial R}{\partial x'})^2 dx'$, and $\int (\frac{\partial^2 R}{\partial x'^2})^2 dx'$ all increase once the filling correction is made. Again, the presence of the local filling effect seems to produce some difficulty when it is combined with a nonlocal advection scheme. It is also interesting to note

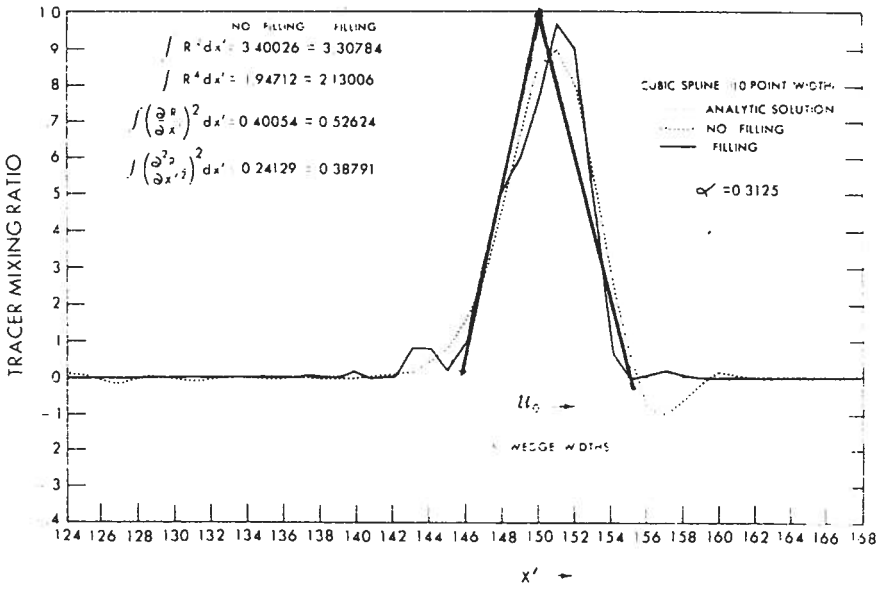

FIGURE 6. Same as Figure 2, except for fourth-order cubic spline algorithm (10 point width each side of grid point i).

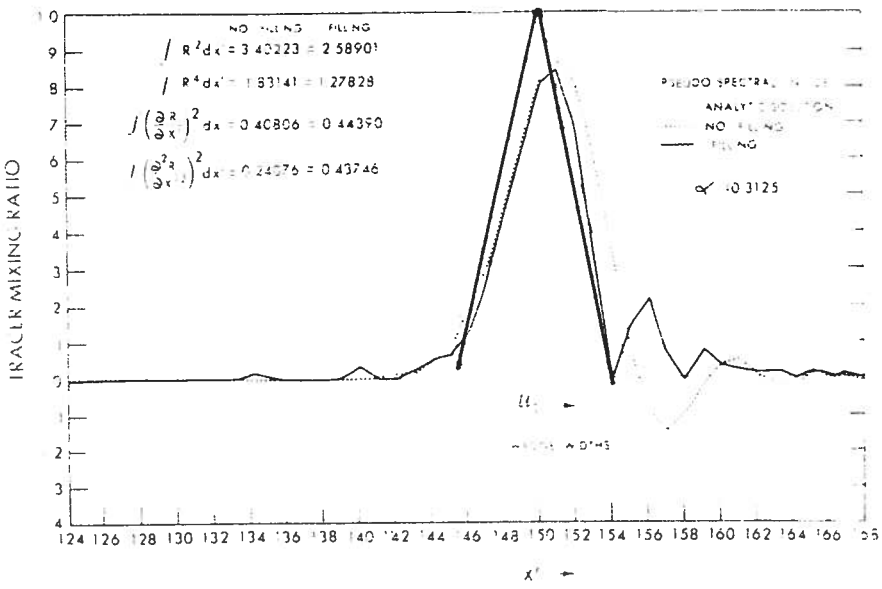

FIGURE 7. Same as Figure 2, except for pseudo-spectral algorithm (n = 128).

that addition of filling to the spline scheme causes the peak mixing ratio to be better preserved than in the no-filling spline experiment. The cause of this is not presently understood.

D. Pseudo-Spectral Algorithms

Results for the pseudo-spectral scheme at α = 0.3125 and n = 128 are shown in Figure 7. The overall appearance of the no-filling run is quite similar to the cubic spline results shown in Figure 6. A hole of -0.14 appears in front of the wedge and a slight phase advance is observed. At first glance, it is rather surprising that this pseudo-spectral experiment shows no properties that are clearly superior to the basic fourth-order results shown in Figure 4.

The filling case in Figure 7 shows a serious distortion by creation of large amplitude, nonphysical bumps. Again, the local filling and a higher-order, nonlocal advection calculation appear to result in an unfavorable interaction. To test this hypothesis, the fourth-order polynomial derivative (Figure 4) and pseudo-spectral n = 128 (Figure 7) experiments were rerun with another filling scheme that was somewhat less local in its formulation. In this trial filling scheme, the negative mixing ratios are still reset to zero each time step; but the borrowing from positive values is not local as is in the original filling scheme. Instead, the net average negative deficit is distributed equally over all 256 grid points. Thus all points serve as donor points, not just the ones adjacent to the negative values. It should be noted here that this type of filling does not totally eliminate negative mixing ratios; however, the holes remaining after its application are uniform and extremely small, about -0.00003.

Results using this revised filling method in the fourth-order polynomial derivative scheme are essentially identical

with the result shown in Figure 4. However, application of this filling scheme to the n = 128 pseudo-spectral result shown in Figure 7 indicates a rather significant change (not shown). The nonphysical bumps seen in Figure 7 are diminished in amplitude by about a factor of 4. However, the magnitude of the peak value decreases by about 5 percent. Thus application of a less local filling scheme significantly reduces the severity of the filling-advection interference so evident in Figure 7.

In pseudo-spectral algorithms, the quantity of wave numbers utilized in a problem is normally much smaller than the 128 wave numbers employed here. Thus for the sake of comparison, the n = 128 pseudo-spectral experiment shown in Figure 7 was repeated but with n = 32. The results for this experiment are shown in Figure 8. The no-filling case is not very dissimilar to that shown in Figure 7. The magnitude of the peak mixing ratio is slightly smaller, and the presence of nonphysical waves on each side of the wedge is more evident.

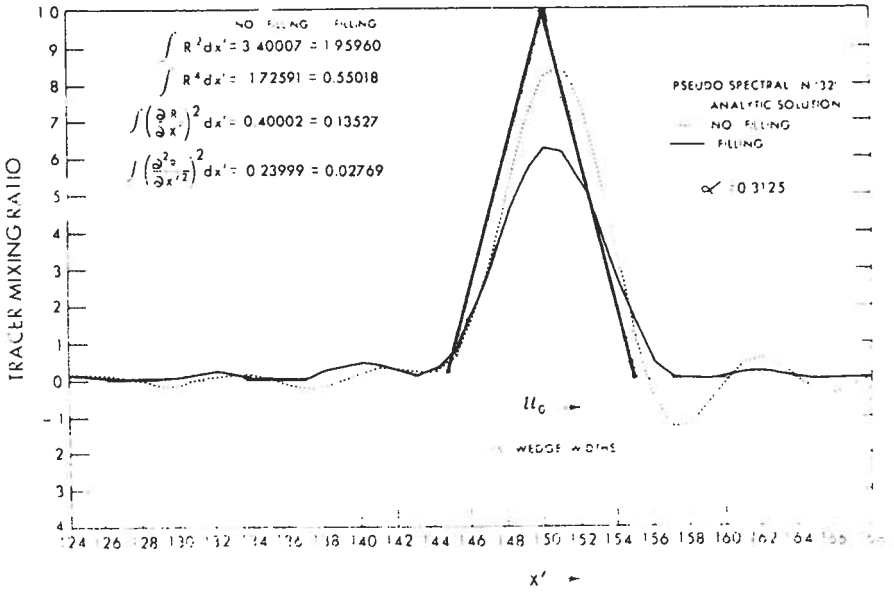

FIGURE 8. Same as Figure 2, except for pseudo-spectral algorithm (n = 32).

The filling case illustrated in Figure 8 shows that the magnitude of the peak mixing ratio diminishes significantly relative to its n = 128 counterpart in Figure 7. Also, the non-physical bumps are not as large as those of the filling case in Figure 7, presumably because it is the shortest wavelengths that interact the most unfavorably with the local filling scheme. This point will be made clearer in Section VI.F.

E. Comparisons at Shorter Time Steps

The performance of the pseudo-spectral scheme is disappointing in view of the remarkably accurate results obtained by Orszag (1971) for a similar advection problem. To gain a better insight into the cause of this discrepancy, the n = 128 pseudo-spectral case is rerun at a much shorter time step (α = 0.03125). The result given in Figure 9 now shows an extremely

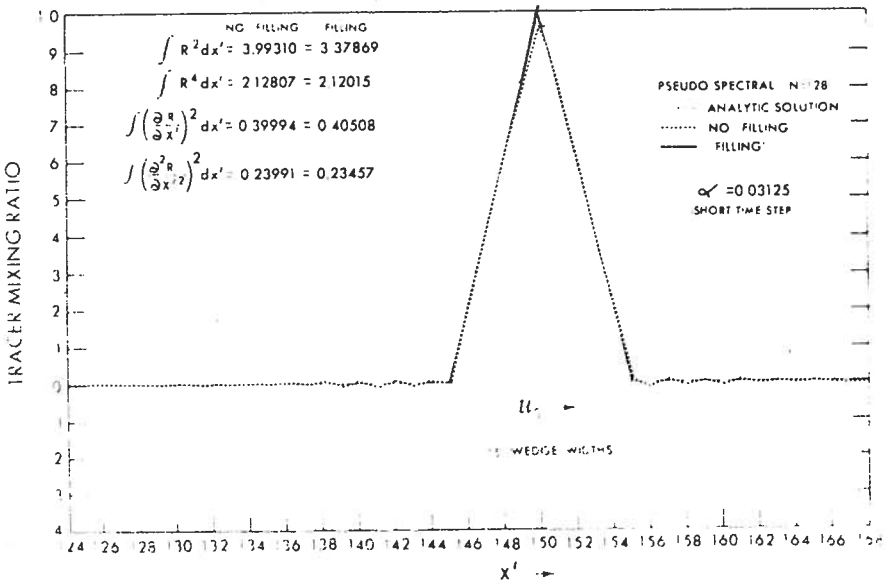

FIGURE 9. Same as pseudo-spectral solution shown in Figure 7, except that the time step has been decreased by a factor of 10 (α = 0.03125).

accurate simulation of the analytic solution, so close in fact, that it is difficult to distinguish them on the graph. The very great contrast in the quality of the solution in Figure 9 compared to the $\alpha = 0.3125$ case in Figure 7 demonstrates the great importance of reducing time-truncation error if accurate advection characteristics are desired in the pseudo-spectral scheme. In short, the pseudo-spectral scheme gives highly accurate results for simple problems of this nature provided the investigator is willing to pay the heavy increase in computing costs required to calculate accurate space derivatives and use very short time steps. For this experiment, the filling case is negligibly different from the no-filling case shown in Figure 9.

For the sake of comparison with Figure 9, the fourth-order derivative scheme illustrated in Figure 4 is also rerun at the much shorter time step ($\alpha = 0.03125$) and shown in Figure 10.

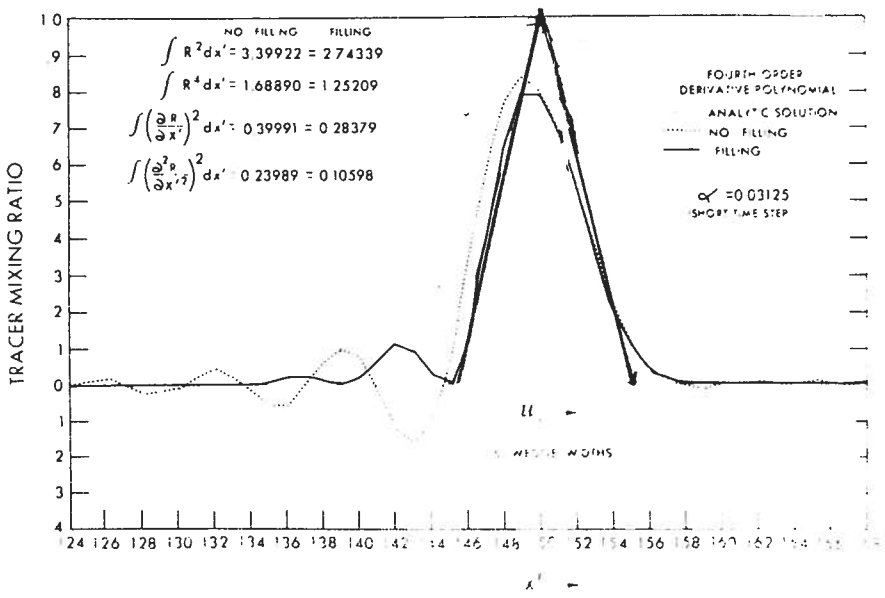

FIGURE 10. Same as fourth-order derivative polynomial solution of Figure 4, except that the time step has been decreased by a factor of 10 ($\alpha = 0.03125$).

It is interesting to note that the results for the $\alpha = 0.03125$ case are worse than those for the $\alpha = 0.3125$ case shown in Figure 4. Observe that there is now a noticeable lag of the peak mixing ratio behind the analytic solution, whereas there was none in the longer time step case. This is because in the $\alpha = 0.3125$ case seen in Figure 4, the well-known phase lag due to space-truncation error is nearly compensated by a phase advance resulting from time-truncation error. Thus when the time step is significantly reduced, these two effects no longer tend to compensate each other.

It is also interesting to note that the peak mixing ratio in Figure 10 is no longer as well preserved as its counterpart in Figure 4. The shorter time step run exhibits more damping of higher-order integrals, and the holes of negative mixing ratio are now deeper. The fact that the filling case for $\alpha = 0.03125$ shows a larger nonphysical bump behind the main wedge of tracer suggests that this bump phenomenon seen in Figures 4 and 10 results from an unfavorable interaction between filling and space-truncation error. On the other hand, the strong contrast between the results given in Figures 7 and 9 suggests that the bump in the pseudo-spectral results is due to an interaction between filling and time-truncation error.

Thus two schemes, which appear to be very similar at intermediate time steps ($\alpha = 0.3125$), differ drastically when calculated at very short time steps ($\alpha = 0.03125$). This implies that the optimum choice of an advection scheme is very strongly dependent upon the investigator's objectives and computing constraints in the problem of interest.

F. Power Spectra

In the discussions of results given in the previous sections, the behavior of the higher-order integrals (6) through (9) was emphasized for various schemes. It was seen that the integrals $\int R^2 dx'$, $\int (\frac{\partial R}{\partial x'})^2 dx'$, and $\int (\frac{\partial^2 R}{\partial x'^2})^2 dx'$ were conserved for the no-filling runs for all algorithms tested except for the fourth-order quasi-Lagrangian scheme. It is also true that the initial spectral distributions of these quantities are preserved in all but the quasi-Lagrangian cases. However, when negative mixing ratio filling is included in the various algorithms, a number of significant effects are observed in the power spectra, particularly in the higher wave numbers.

Although the power spectra of R^2, $(\frac{\partial R}{\partial x'})^2$, and $(\frac{\partial^2 R}{\partial x'^2})^2$ were

all calculated for each algorithm tested, the spectra of $(\frac{\partial^2 R}{\partial x'^2})^2$ were chosen for presentation. Basically, the spectra of each of these quantities lead to similar interpretations, but the results are more obvious in the spectra of $(\frac{\partial^2 R}{\partial x'^2})^2$. Also, this quantity is particularly interesting because its spurious amplification at a given wave number signals that explicit diffusive effects might be required to prevent the amplification from becoming disastrous.

Figure 11 shows calculated power spectra of $(\frac{\partial^2 R}{\partial x'^2})^2$ (approximated by $(R_{i+1} - 2R_i + R_{i-1})^2$) for: the initial condition (Figure 1); the second-order polynomial algorithm (Figure 2); the fourth-order derivative polynomial algorithm (Figure 4); and the pseudo-spectral algorithm (Figure 7). All three cases shown are with filling and for $\alpha = 0.3125$. Note that the spectrum of $(\frac{\partial^2 R}{\partial x'^2})^2$ for the initial condition shows considerable power at the higher wave numbers; the maxima occur at about n = 25 and n = 80, with the same magnitude.

In the numerical integrations, the growth of noise and smaller-scale structure in the grid itself is of great interest. Figure 11 shows that filling in the second-order polynomial scheme has led to severe damping in the intermediate and high wave numbers. The high wave number damping has thus significantly acted to "smooth" out the spectrum. This is closely analogous to the effect of adding a nonlinear diffusion term to the advection problem.

As might have been anticipated from previous discussions on the results presented in Figures 2 through 10, the spectra for the higher-order schemes with filling are very different from that of the second-order polynomial scheme. Figure 11 shows that the spectrum from the fourth-order derivative polynomial algorithm with filling is very similar to that of the initial condition up to about n = 25. However, from about n = 25 to n = 60 the amount of power has increased. This is a spurious amplification that was excited by the introduction of filling to the solution. In the higher wave numbers (n > 60), damping due to filling is evident. Overall, the damping effect dominates the solution since $\int(\frac{\partial^2 R}{\partial x'^2})^2 dx'$ diminishes with the addition of filling to this algorithm (see Figure 4).

The power spectrum of $(\frac{\partial^2 R}{\partial x'^2})^2$ in Figure 11 for the pseudo-spectral algorithm (results shown in Figure 7) reveals a very

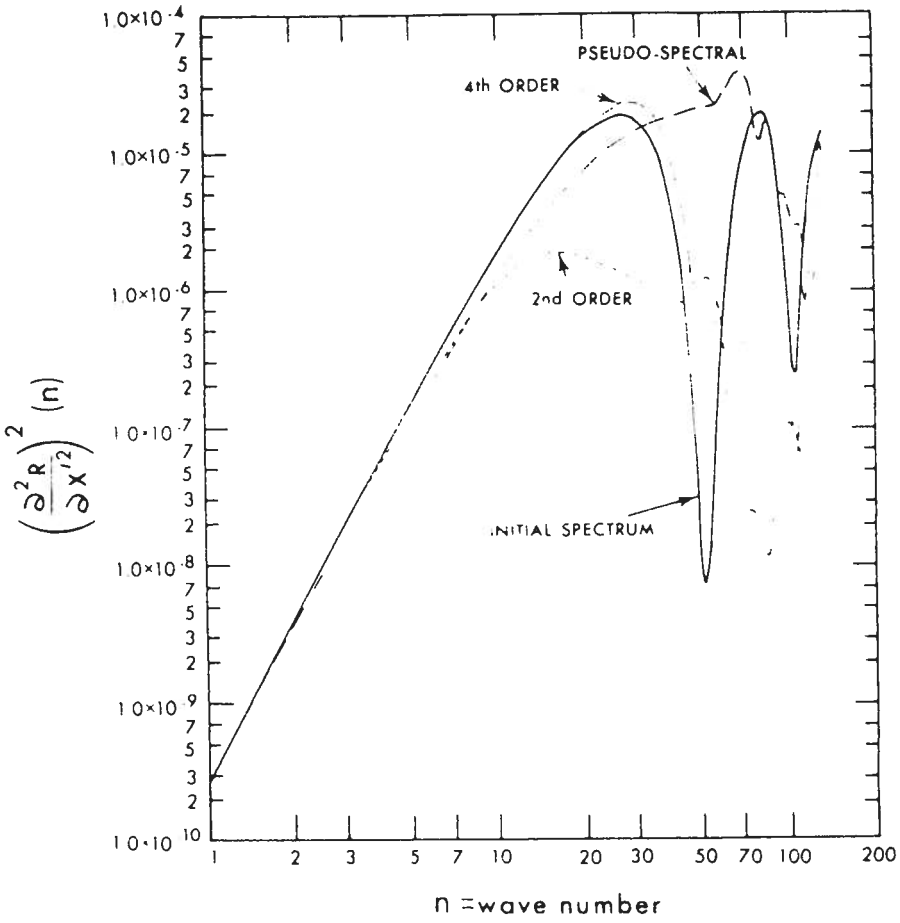

FIGURE 11. Power spectra of $(\frac{\partial^2 R}{\partial x'^2})^2$ (n) for α = 0.3125 cases with filling for: initial condition, second-order polynomial algorithm, fourth-order polynomial algorithm, and pseudo-spectral algorithm.

different behavior than observed in the other cases. A significant damping of $(\frac{\partial^2 R}{\partial x'^2})^2$ (n) relative to the initial spectrum can be seen from n = 1 to about n = 30. However, above n = 30 a very pronounced amplification has occurred relative to the initial spectrum. This effect is particularly evident for the interval n = 65 through n = 70, which shows over twice the power per wave number than was previously present at any wave number in the initial spectrum.

Such a spurious amplification at higher wave numbers is potentially serious because it indicates that [illegible] higher wave numbers occurred purely as a result of time-truncation error interacting with filling. Furthermore, the high-wave number amplification is greater than the low-wave-number damping since $\int(\frac{\partial^2 R}{\partial x'^2})^2 dx'$ is increasing with time as can be seen in Figure 7. Thus even though the pseudo-spectral algorithm showed superior properties at very small α, it may be the most susceptible to an unfavorable interaction with highly localized processes in problems of this type.

G. Boundary Interference

As pointed out earlier, all the algorithms tested employed cyclic boundary conditions in a limited domain (NI = 256). However, all schemes tested show the presence in the solutions of structure that is nonphysical and that exists some distance from the correct location of the main wedge. Thus an obvious question is whether or not the nonphysical parts of the numerical solution act in any way to produce a self-contamination of the remaining "good" part of the solution. A straightforward way to test this effect is by using the standard second-order polynomial method, since its computational effects are well known.

The second-order scheme, the results of which are shown in Figure 2, was used to advect the wedge on the usual NI =256 grid for a distance of 90 wedge widths or 900 grid points. Then, the identical case was run, but with an expanded grid of NI = 1024. The results of this comparison are shown in Figure 12. Both solutions show again the obvious deficiencies of the second-order algorithm. However, the physical appearances of the two solutions are quite different. The run with NI = 1024 is relatively smooth in appearance, while the NI = 256 case shows noticeable irregularities. This is true in spite of the fact that all integrals and all spectra are virtually identical in the two experiments.

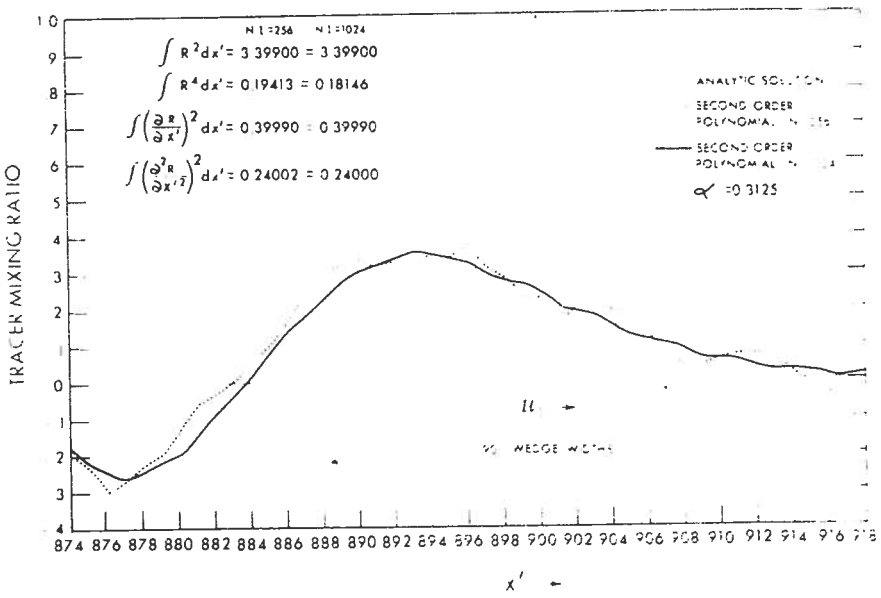

FIGURE 12. Comparison of two no-filling experiments with the second-order polynomial algorithm at NI = 256 and NI = 1024.

The differences shown in Figure 12 are entirely due to self-contamination because the longest wavelengths are moving at nearly the speed u_o, whereas the shortest wavelengths experience a severe lag. Thus at very long integration times, the faster moving lower frequencies tend to overlap the nonphysical trail of disturbances behind the main wedge.

If filling is added to this test, the solutions at NI = [illegible] and NI = 1024 look virtually identical (not shown). This is because the higher frequency effects are now severely suppressed, as can be seen in Figures 2 and 11.

VII. CONCLUSIONS

A simple, linear, one-dimensional trace constituent advection problem is solved numerically for the purpose of testing

the relative merits of various numerical algorithms. The algorithms reported here fall into four basic categories depending upon the approach employed: polynomial, quasi-Lagrangian, cubic spline, and pseudo-spectral algorithms.

Of the polynomial algorithms tested, the standard second-order scheme shows some serious deficiencies. The standard fourth-order derivative scheme demonstrates a substantial improvement, even though significant discrepancies remain. The fourth-order flux divergence scheme shows results intermediate between the standard second- and fourth-order schemes.

The fourth-order quasi-Lagrangian and cubic spline algorithms do not demonstrate any significant improvement over the standard fourth-order polynomial derivative scheme. This is the case in spite of a substantial increase in computation time and programming complexity required to use either of these algorithms.

By far the most successful results were obtained with the pseudo-spectral method. This approach yielded a nearly exact correspondence with the analytic solution. However, these results are achieved at a higher computing cost because many wave numbers and very small time steps are required before high accuracy is realized.

In each of the algorithms, space- and/or time-truncation error can lead to prediction of nonphysical negative mixing ratios. The effect of "correcting" these negative mixing ratios to nonnegative values was tested in each algorithm by incorporating a tracer-conserving filling scheme. In general, the physical appearance of the computed solutions was improved by including this correction. In the second-order polynomial scheme, this improvement occurs at the expense of severe damping of all higher-order integrals. In the higher-order advection schemes, with the addition of filling $\int R^2 dx'$ continues to be damped, but a spurious amplification occurs in the higher-order integrals. This is especially true in pseudo-spectral schemes, where the power spectrum of $(\frac{\partial^2 R}{\partial x'^2})^2$ shows fictitious increases at very high wave numbers. Additional experiments were run with a negative mixing ratio filling that is less local in its behavior. The results show that the spurious amplification in higher wave numbers can be reduced somewhat with care in the choice of a filling scheme.

ACKNOWLEDGMENTS

The authors are indebted to M. Suarez, who generously assisted us with the cubic spline routine; to H. Kaufman for considerable technical assistance; and to L. J. Polinsky, who graciously helped us with his graphing routines. Special appreciation is also extended to Y. Kurihara, J. L. Holloway, Jr., and C. T. Gordon for helpful discussions and very useful comments on the manuscript.

REFERENCES

1. Ahlberg, J. H., Nilson, E. N., and Walsh, J. H. 1965. J. Math. Anal. Appl. 12, 27.

2. Ahlberg, J. H., Nilson, E. N., and Walsh, J. H. 1967. The Theory of Splines and Their Applications, Academic, New York.

3. Bryan, K. 1966. Mon. Weather Rev. 94, 39.

4. Burnstein, S. Z. and Mirin, A. A. 1970. J. Comput. Phys. 5, 547.

5. Cooley, J. W. and Tukey, J. W. 1965. Math. Comp. 19, 297.

6. Crowley, W. P. 1967. J. Comput. Phys. 1, 471.

7. Crowley, W. P. 1968. Mon. Weather Rev. 96, 1.

8. Cunnold, D., Alyea, F., Phillips, N., and Prinn, R. 1975. J. Atmos. Sci. 32, 170.

9. de Boor, C. 1962. J. Math. Phys. 41, 212.

10. Fritsch, J. M. 1971. Mon. Weather Rev. 99, 379.

11. Hunt, B. G. and Manabe, S. 1968. Mon. Weather Rev. 96, 503.

12. Krishnamurti, T. N. 1962. J. Appl. Meteor. 1, 508.

13. Kurihara, Y. and Holloway, J. L., Jr. 1967. Mon. Weather Rev. 95, 509.

14. Lawrence-Livermore Laboratory. 1974. Development of an Air Pollution Model for the San Francisco Bay Area, Second Semiannual Report to the National Science Foundation, UCRL-51537.

15. Lax, P. D. and Wendroff, B. 1960. Systems of Conservation Laws, Communications on Pure and Applied Mathematics, vol. 13, pp. 217-237, Interscience, New York.

16. Leith, C. E. 1965. Numerical Simulations of the Earth's Atmosphere, Methods in Computational Physics, Applications in Hydrodynamics, vol. 4, pp. 1-28, Academic, New York and London.

17. Mahlman, J. D. 1973. Preliminary Results from a Three-Dimensional, General-Circulation Tracer Model, Proceedings of the Second Conference on the Climatic Impact Assessment Program (A. J. Broderick, ed.), 1st edition, pp. 321-337.

18. Mathur, M. B. 1970. Mon. Weather Rev. 98, 214.

19. Molenkamp, C. R. 1968. J. Appl. Meteor. 7, 160.

20. Orszag, S. A. 1971. J. Fluid Mech. 49, 75.

21. Orszag, S. A. 1972. Stud. Appl. Math. 51, 253.

22. Orszag, S. A. and Jayne, L. W. 1974. J. Comput. Phys. 14, 93.

23. Price, G. V. and MacPherson, A. K. 1973. J. Appl. Meteor. 12, 1102.

24. Reiter, E. R. 1972. Atmospheric Transport Processes, Hydrodynamic Tracers, Part 3, AEC Critical Review Series, U. S. Atomic Energy Commission, Office of Information Services.

25. Richtmeyer, R. D. 1963. A Survey of Difference Methods for Nonsteady Fluid Dynamics, NCAR Technical Note 63-2, National Center for Atmospheric Research, Boulder, Colorado.

On the Interfacing of Chemical, Physical, and Biological Water Quality Models

F. M. MOREL AND J. G. YEASTED
Ralph M. Parsons Laboratory
for Water Resources and Hydrodynamics
Department of Civil Engineering
Massachusetts Institute of Technology
Cambridge, Massachusetts

I. INTRODUCTION

The ultimate goal of building a model is to be able to predict the outcome of a complex phenomenon. A more modest but equally worthwhile purpose for model building is to gain some understanding of a phenomenon, or to identify critical parameters and processes. In the water quality field, the necessity to make engineering and policy decisions creates a great demand for predictive models. As a result, models that were not intended to be predictive are used as such, and a certain distrust of all water quality models arises. A clear statement of the purpose for all models would help to alleviate this situation.

One of the reasons why water quality models are rarely predictive is that they reflect the expertise of their builders in being sophisticated in one aspect and hopelessly crude in others, as for example, chemists dealing with well-mixed systems, hydrodynamicists considering all substances to be conservative